Appl. Phys. A 69 [Suppl.], S869–S873 (1999) / Digital Object Identifier (DOI) 10.1007/s003399900316

Applied Physics A
Materials
Science & Processing

Interface kinetics during pulsed laser ablation

X. Xu*, K. Song

School of Mechanical Engineering, Purdue University, West Lafayette, IN 47907-1288, USA
(Fax: +1-765/494-0539, E-mail: xxu@ecn.purdue.edu)

Received: 21 July 1999/Accepted: 1 September 1999/Published online: 28 December 1999

Abstract. This work investigates evaporation kinetics — the relation between the surface temperature and pressure during excimer laser ablation. Nickel targets are ablated by excimer laser pulses in a laser fluence range between 1 and 6 J/cm^2, with the upper limit exceeding the threshold of phase explosion (5 J/cm^2). The surface pressure is determined with a polyvinylidene fluoride (PVDF) piezoelectric transducer. When phase explosion occurs, the surface temperature is known to be near the thermodynamic critical temperature, therefore, by measuring the surface pressure, the surface temperature-pressure relation is determined at the threshold fluence of phase explosion. The surface temperature and the threshold fluence of phase explosion are also estimated from the measured velocity of the vapor plume and gas dynamics calculations. It is shown that, during excimer laser ablation, the temperature and pressure relation deviates significantly from the equilibrium kinetic relation.

PACS: 79.20.Ds; 68.10.Jy; 68.35.Rh

This work investigates the kinetics at the evaporating surface during excimer laser ablation. The relation between the transient surface temperature and the transient surface pressure, which determines the evaporation mechanism and the evaporation rate, is of prime interest. It is known that during laser ablation superheating in the liquid could occur. When the liquid is superheated to the limit of thermodynamic stability, the spinodal point, an explosive type of phase change termed "phase explosion" or "explosive phase change" occurs [1]. The explosive phase change has been observed experimentally during nanosecond pulsed excimer laser ablation of nickel at laser fluences higher than 5 J/cm^2 [2]. Using a numerical procedure, it is also shown that at laser fluences higher than 5 J/cm^2 the surface temperature of nickel reaches the spinodal point [3].

It has also been suggested that during the evaporation process induced by a pulsed excimer laser, the surface temperature-pressure relation does not follow the binode or the Clausius–Clapeyron relation. However, to date there has been no report in the literature of experimental studies of the actual surface temperature-pressure relation during laser ablation. It has been common practice to use the equilibrium Clausius–Clapeyron relation to compute the surface pressure and the evaporation rate. The present work is intended to determine the deviation of the surface temperature-pressure relation from the Clausius–Clapeyron relation experimentally. The surface pressure is measured with the use of a thin polyvinylidene fluoride (PVDF) transducer (K-tech Co., Albuquerque, NM). The surface temperature is known to be near the spinodal temperature ($\sim 0.9\,T_c$, where T_c is the thermodynamic critical temperature) when phase explosion occurs. However, measurements of the surface temperature are not attempted since the plasma plume produced by laser ablation disrupts any information coming out from the surface. Instead, the surface temperature is estimated from a gas dynamics calculation using the measured velocity of laser-evaporated vapor as the input parameter. Using these approaches, the surface temperature-pressure relation is reconciled. The experiments are performed in a laser fluence range between 1 and 6 J/cm^2, with the lower end near the evaporation threshold and the upper end exceeding the threshold of phase explosion.

1 Pressure measurement with the PVDF transducer

The PVDF transducer is a well-established technique to study pressure in solids. There are also a number of studies on using the PVDF transducer to measure stress waves in solids produced by laser irradiation [4-6]. The PVDF transducer offers many advantages in stress measurements, including fast time resolution ($\sim$ 1 ns), large measurement range (0.1 bar to 10 Mbar), and large signal output. In addition, PVDF transducer signals are highly reproducible under recurrent shock loading, which is often lacking in conventional piezoelectric shock sensors. The properties and responses of PVDF transducers to pressure have been well characterized [7]. Under shock loading, the PVDF transducer delivers a voltage, $V(t)$, proportional to the stress difference between the two surfaces

*Corresponding author.

COLA'99 – 5th International Conference on Laser Ablation, July 19–23, 1999 in Göttingen, Germany

of the PVDF transducer foil [8]

$$V(t) = \frac{d_{33} D_s A R}{l} [\sigma_f(t) - \sigma_b(t)] \,, \quad (1)$$

where d_{33}, D_s, A, R, and l are, respectively, the piezoelectric constant, the shock velocity, the active area of the transducer, the terminal resistance load, and the transducer thickness. $\sigma_f(t)$ and $\sigma_b(t)$ are, respectively, the pressure history at the front and back faces of the transducer. The values of A and l of the PVDF sensor used in this work are, respectively, 1.05 mm^2 and 21.60 μm. When the stress applied to the transducer is less than 30 MPa, d_{33} is 15.7 pC/N [9]. The transducer is custom-built and calibrated by K-tech Co.

The experimental setup is illustrated in Fig. 1. The laser used in this work is a KrF excimer laser ($\lambda = 248$ nm) with a 30 ns pulse width (FWHM). A CaF_2 lens with a 150 mm focal length is used to focus the laser beam on the target. In order to limit the two-dimensional shock wave propagation effect, the laser spot size needs to be larger than the thickness of the target foil, and also larger than the active area of the PVDF transducer (1 mm × 1 mm). In this experiment, the size of the laser spot is varied between 0.065 cm^2 (1.8 mm × 3.6 mm) and 0.25 cm^2 (3.5 mm × 7.0 mm). The energy per laser pulse at the target surface is calibrated using an energy meter. Energy fluctuation is monitored using a built-in energy meter of the excimer laser, which is found to be less than 3%. A fast silicon photodiode sensing a split beam from the excimer laser beam is used to trigger the data acquisition system.

Figure 2 shows the detailed assembly of the target and the PVDF transducer. The target is a 242 μm thick nickel foil with 99.95% purity. Before taking data at a laser fluence, the target surface is pre-treated using multiple laser pulses at that laser fluence. A 1.047 mm thick Kel-F (polychlorotrifluoroethylene) buffer and thin adhesive Teflon (polytetrafluoroethylene) resin (51 μm thick) hold the nickel target to the PVDF transducer. The shock impedance of Kel-F and Teflon is matched with that of the PVDF transducer. A 25.5 mm thick Kel-F backer is used to mount the PVDF transducer, and the whole transducer assembly is housed in an aluminum canister, which is 25 mm in diameter and 50 mm long. The PVDF transducer is connected to a digital storage oscilloscope (Tektronix TDS744), which is set to the 50 Ω terminal load resistance for fast data acquisition.

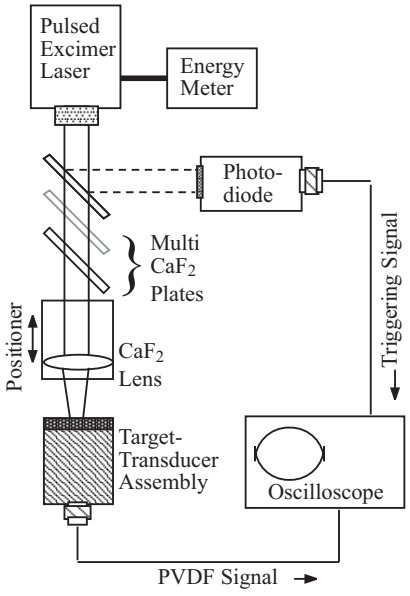

Fig. 1. Experimental setup

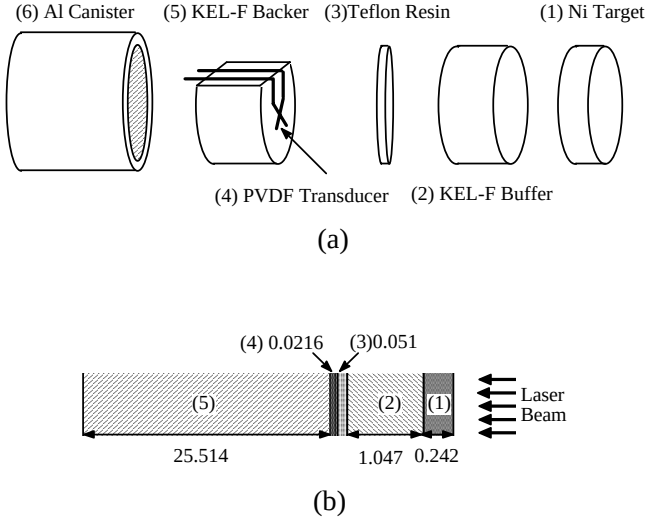

Fig. 2a,b. Detailed target and PVDF transducer assembly. **a** Components of a PVDF transducer; **b** dimensions of each component (mm)

Before the laser-produced shock reaches the back surface of the PVDF transducer, the stress at the back surface of the PVDF transducer, σ_b, is zero. Therefore, from (1), the output voltage signal is directly proportional to the stress at the front of the PVDF transducer, σ_f. As the shock wave reaches the back surface of the PVDF transducer, σ_b starts to decrease. The time for the shock to pass through the PVDF transducer, τ, is about 10 ns. When the shock reaches the back of the PVDF transducer, the recorded voltage signal is proportional to $[\sigma_f(t) - \sigma_b(t)]$, where $\sigma_b(t) = \sigma_f(t - \tau)$. It is assumed that attenuation of the shock wave from the front to the back surface of the PVDF transducer is negligible. This is due to the small thickness of the PVDF transducer, and the low shock pressure, which is not enough to generate considerable heating. Experimental justifications of this assumption will be seen later. When the shock reaches the back surface of the PVDF transducer, the value of $\sigma_f(t)$ can be calculated as

$$\sigma_f(t) = \frac{V(t) l}{d_{33} D_s A R} + \sigma_f(t - \tau) \,. \quad (2)$$

The recorded voltage signal from the oscilloscope can be converted to the pressure at the PVDF transducer using (2).

The shock impedance mismatch method is used to obtain the stress profile in the nickel target from the measured stress profile in PVDF. Since the shock impedances of Teflon and KEL-F are the same as that of PVDF, there is only one reflection of the shock wave at the back side of the nickel. The total thickness of the material behind the nickel foil is large, so that the reflection of shock waves from the free end of the KEL-F backer does not need to be considered. The transmitted wave into the Teflon resin is a compression shock wave, and the reflected wave into the nickel foil is a rarefaction wave since the dynamic rigidity of Teflon is smaller than that of nickel.

In order to determine the stress in nickel from the measured stress in PVDF, stress-particle velocity (σ-u) relations of nickel and PVDF (or Teflon) are needed, which can be determined from the Hugoniot data [10]. According to the conservation of momentum across the shock wave front, the stress σ and the particle velocity u are related as

$$\sigma = \varrho_0 D u \,, \tag{3}$$

where ϱ_0 and D are, respectively, the density and shock velocity, with the subscript 0 denoting the state ahead of the shock. In this work, the stress produced by laser irradiation is rather small; therefore shock velocities can be treated as constants, as for the shock impedance ($\varrho_0 D$) of nickel and PVDF. Using conservation of momentum, the particle velocity in nickel can be calculated as

$$u_{\mathrm{Ni}} = \frac{\sigma_{\mathrm{PVDF}} + (\varrho_0 D)_{\mathrm{Ni}} u_{\mathrm{PVDF}}}{2(\varrho_0 D)_{\mathrm{Ni}}} \tag{4a}$$

and the stress in nickel can be calculated as

$$\sigma_{\mathrm{Ni}} = (\varrho_0 D)_{\mathrm{Ni}} u_{\mathrm{Ni}} \,. \tag{4b}$$

Using (1)–(4), the measured PVDF output can be converted to the pressure in PVDF and the pressure in the nickel target. Detailed descriptions of the above calculations have been presented elsewhere [11].

2 Surface temperature measurement

The surface temperature is known to be near the critical temperature at the threshold fluence of phase explosion, $5\,\mathrm{J/cm^2}$ [2]. At other laser fluences, the surface temperature is estimated from the measured plume propagation velocity using a gas dynamics analysis. The measurement of the plume velocity has been presented elsewhere [2], and will not be repeated here.

The gas dynamics model used in this work follows that given by Knight [12]. When the laser fluence is higher than the ablation threshold but less than the threshold for phase explosion, the flow process can be depicted as Fig. 3a. The laser-evaporated vapor leaves the target surface with a half Maxwellian distribution. Collisions in the vapor establish thermodynamic equilibrium in the Knudsen layer. On leaving the Knudsen layer, the vapor experiences an expansion, compressing the air ahead of the vapor at the contact front. The compressed air propagates into the ambient air, forming a shock wave. When the laser fluence is higher than the threshold of phase explosion, the superheated liquid turns into a mixture of liquid and vapor propagating into the air, as shown in Fig. 3b. The mixture also forms a contact front with the air, and the compressed air propagates into the ambient, forming a shock.

Based on the surface evaporation model described above (Fig. 3a), it is possible to relate the measured velocity of the shock wave to the temperature at the surface. The velocity of the shock wave, v_{sh}, is related to the temperature and velocity behind the shock, T_{ca}, and v_{ca}, by the Hugoniot equation [13] as

$$\frac{T_{\mathrm{ca}}}{T_{\mathrm{amb}}} = \frac{(2\gamma_{\mathrm{air}} M_{\mathrm{sh}}^2 - (\gamma_{\mathrm{air}} - 1))((\gamma_{\mathrm{air}} - 1) M_{\mathrm{sh}}^2 + 2)}{((\gamma_{\mathrm{air}} + 1) M_{\mathrm{aa}})^2} \tag{5a}$$

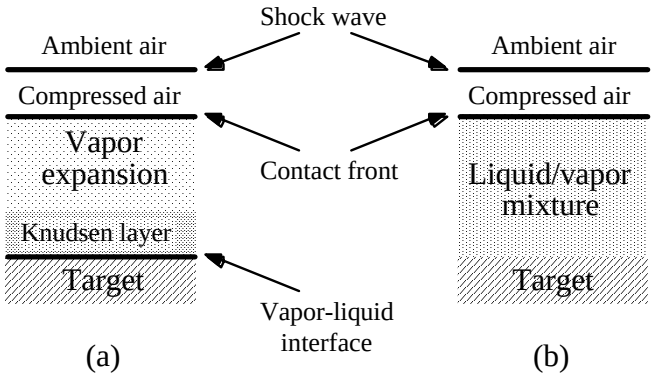

Fig. 3a,b. One-dimensional gas dynamic models: **a** surface evaporation; **b** explosive phase change

$$\frac{v_{\mathrm{ca}}}{v_{\mathrm{sh}}} = \frac{\gamma_{\mathrm{air}} - 1}{\gamma_{\mathrm{air}} + 1} + \frac{2}{\gamma_{\mathrm{air}} + 1 M_{\mathrm{sh}}^2} \tag{5b}$$

M_{sh} is the Mach number of the shock. $\gamma_{\mathrm{air}} = 1.4$ is the ratio of specific heats of air.

It is assumed that the pressure, temperature, and velocity are uniform in the compressed air. At the contact front, the pressure, temperature, and velocity of Ni vapor, p_{cf}, T_{cf}, and v_{cf}, are the same as those of the compressed air. The relation between the temperature at the contact front and that at the exit of the Knudsen layer, T_{KL}, is

$$c_{\mathrm{p}} T_{\mathrm{cf}} + 0.5 v_{\mathrm{cf}}^2 + P_{\mathrm{abs}} = c_{\mathrm{p}} T_{\mathrm{KL}} + 0.5 v_{\mathrm{KL}}^2 \tag{6}$$

where c_{p} is the specific heat of nickel vapor and P_{abs} is the laser power absorbed by the plume. For the laser fluence used in this work, it has been shown that the Mach number at the exit of the Knudsen layer is 1 [14]. Therefore the velocity at the exit of the Knudsen layer is the local sonic velocity, and is determined by the local temperature.

The conservation equations of mass, momentum and energy are used to establish the relationship between the thermodynamic properties at the target surface and at the exit of the Knudsen layer. When the Mach number at the exit of the Knudsen layer is 1, the following relation applies [12]:

$$T_{\mathrm{KL}} = 0.669\, \mathrm{T_{sur}} \,. \tag{7}$$

Using (5)–(7), along with the measured shock velocity and absorption of laser power by the plume, the temperature at the target surface, T_{sur}, can be estimated. The description of the measurement of absorbed laser power has been presented elsewhere [15].

3 Results and discussion

3.1 Results of the pressure measurement

Figure 4 shows typical signals recorded during the PVDF measurement. The laser fluence is $3.2\,\mathrm{J/cm^2}$. There is a time delay between the triggering signal and the PVDF signal, during which the shock wave travels through the nickel target, the Kel-F buffer, and the Teflon resin. The initial voltage peak is due to the arrival of the incident shock on the front surface

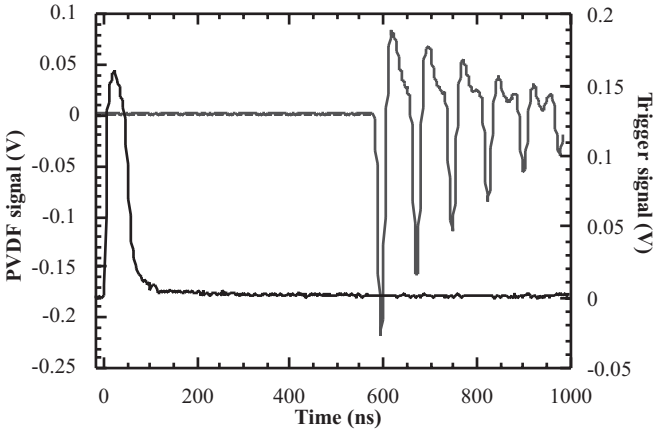

Fig. 4. PVDF signals at $F = 3.2\,\mathrm{J/cm^2}$

of the PVDF transducer. The polarity of this initial signal is negative, indicating that the wave is compressive.

Figure 5 shows the PVDF signal, the calculated stresses in Teflon and PVDF, and the calculated stress in nickel at the laser fluence of $3.2\,\mathrm{J/cm^2}$. The laser pulse is terminated at 50 ns. Periodic recurrences of negative and positive peaks are due to reverberations of the shock wave between the free surface of the nickel target and the nickel-Teflon interface. The period is 78 ns, and it does not change with laser fluence. This indicates that the shock velocity does not decay when the shock travels in nickel. The magnitude of the peak decreases after each round trip between the free surface of nickel and the nickel-Teflon interface, which is due to shock transmission at the nickel- Teflon interface. Figures 5b and 5c show

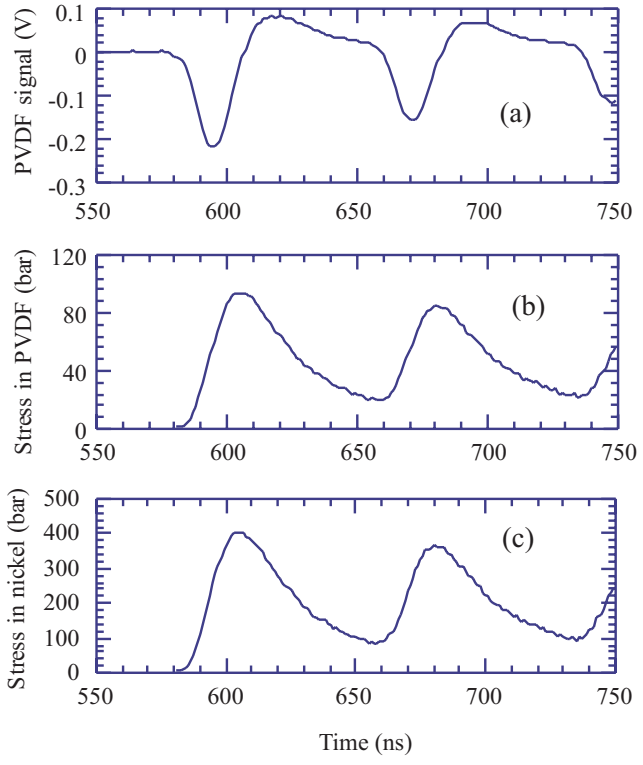

Fig. 5. a PVDF signal; **b** stress in PVDF, and **c** stress in nickel at $F = 3.2\,\mathrm{J/cm^2}$

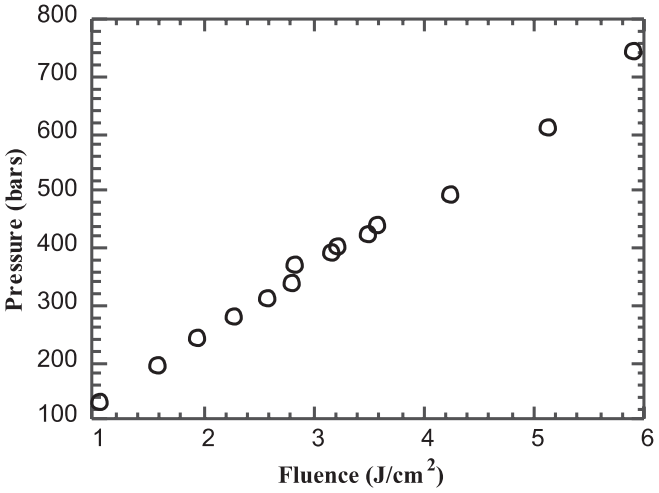

Fig. 6. Peak stress in the nickel target at different laser fluences

the temporal stress profiles in PVDF and nickel calculated from the PVDF signals shown in Fig. 5a. The positive stress denotes compression. The velocity of the shock wave in the nickel target is found to be close to the velocity of the sonic wave; therefore the assumption of negligible attenuation of the shock wave is valid since the propagation of a sonic wave is adiabatic. It is also found that the shock velocity does not change with laser fluence.

Figure 6 shows the peak value of the first compression pulse in nickel as a function of laser fluence. The lowest laser fluence is higher than the ablation threshold value of nickel, which was measured to be $0.9\,\mathrm{J/cm^2}$ [15]. The peak stress increases almost linearly with the laser fluence, from 100 bar to about 760 bar when the laser fluence is increased from 1 to $6\,\mathrm{J/cm^2}$.

3.2 Results of the temperature calculation

The calculated surface temperatures are shown in Fig. 7. At very low laser fluences (less than $2\,\mathrm{J/cm^2}$), the optical signals in the velocity measurements are very weak. Reliable velocity data are obtained at laser fluences of $2.5\,\mathrm{J/cm^2}$ and

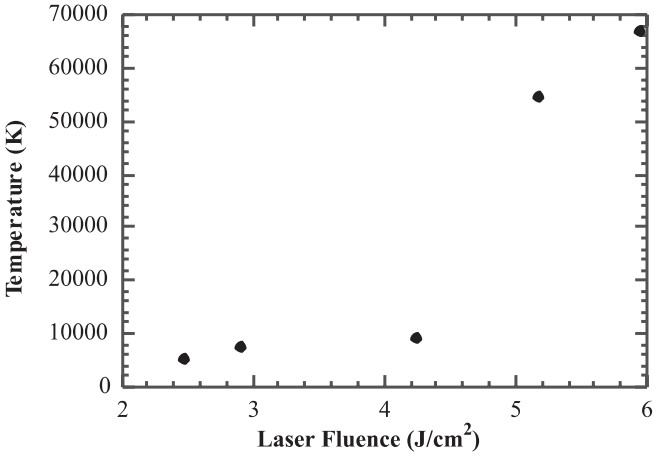

Fig. 7. Peak surface temperature at different laser fluences

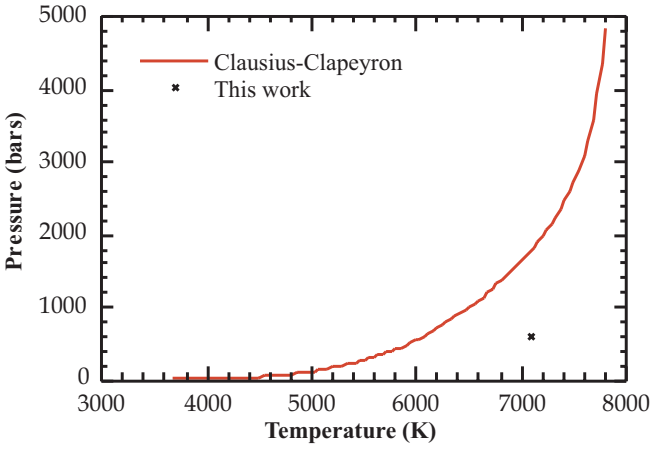

Fig. 8. Comparison between the surface temperature and pressure obtained in this work and the Clausius–Clapeyron relation

higher; therefore temperatures are only calculated at those laser fluences. The calculation shows that the surface temperature at laser fluences below 5 J/cm^2 is around the critical temperature of Ni, 7810 K [16]. It should be noted that the temperature computations carry a large uncertainty due to various assumptions used in the calculation, including steady state flow and constant materials properties. Therefore, from these calculations, determining the surface temperature accurately is unlikely. However, when the laser fluence is above 5 J/cm^2, the calculated temperature at the liquid surface is more than five times higher than the critical temperature. Obviously, such high temperatures cannot exist at the liquid surface. Therefore the computational model used in this work, which is based on surface evaporation, is not applicable to laser ablation with laser fluences higher than 5 J/cm^2, and phase explosion must have occurred at laser fluences higher than 5 J/cm^2. This result agrees with previous studies that the threshold fluence for phase explosion is about 5 J/cm^2 [2].

In Fig. 8, the Clausius–Clapeyron relation for Ni is shown. The critical values of Ni are taken from Martynyuk [16]. Since it is known that explosive phase change occurs at about 5 J/cm^2, the temperature of the surface reaches the spinodal temperature ($\sim 0.9T_c$) at that fluence. The temperature and the pressure at 5 J/cm^2 are also plotted in the figure. It is seen that the temperature-pressure data do not agree with that predicted from the Clausius–Clapeyron relation. The measured pressure is only about 600 bar (Fig. 6), well below the pressure predicted by the Clausius–Clapeyron relation (1800 bar). This shows that, during pulsed laser ablation, the superheated states exist, and the actual surface kinetic relation deviates from the equilibrium Clausius–Clapeyron relation.

4 Conclusions

The time-resolved stress profile during excimer laser ablation of nickel targets was obtained using a polyvinylidene fluoride (PVDF) piezoelectric transducer and impedance mismatch calculation. The peak stress produced by the laser pulse increased almost linearly with laser fluence in the range between 1 and 6 J/cm^2, from 100 bar to about 760 bar. Combined with the temperature for phase explosion, which occurred at about 5 J/cm^2, it was shown that the surface pressure was far less than the pressure predicted by the equilibrium Clausius–Clapeyron equation. The surface temperature-pressure relation during laser ablation deviates significantly from the equilibrium relation.

Acknowledgements. Support for this work by the National Science Foundation (CTS-9624890) is gratefully acknowledged.

References

1. R. Kelly, A. Miotello: Appl. Surf. Sci. **96-98**, 205 (1996)
2. K.H. Song, X. Xu: Appl. Surf. Sci. **127-129**, 111 (1998)
3. X. Xu, G. Chen, K.H. Song: Int. J. Heat Mass Transfer **42**, 1371 (1999)
4. P.E. Dyer, R. Srinivasan: Appl. Phys. Lett. **48**, 445 (1986)
5. L.M. Lee, D.A. Hyndman, R.P. Reed, F. Bauer: In *Shock Compression of Condensed Matter — 1989*, ed. by S.C. Schmidt, J.N. Johnson, L.W. Davison (Elsevier Science Publishers, Oxford 1990)
6. S. Couturier, T. de Resseguier, M. Hallouin, J.P. Romain, F. Bauer: J. Appl. Phys. **79**, 9338 (1996)
7. F. Bauer: Ferroelectrics **115**, 247 (1991)
8. M. Boustie, S. Couturier, J.P. Romain, D. Zagouri, H. Simonnet: Laser Particle Beams **14**, 171 (1996)
9. D.A. Hyndman, E.S. Gaffney: In *Shock Compression of Condensed Matter — 1989*, ed. by S.C. Schmidt, J.N. Johnson, L.W. Davison (Elsevier Science Publishers, Oxford 1990)
10. S.P. Marsh: *LASL Shock Hugoniot Data* (University of California Press, Berkeley 1980)
11. K.H. Song, X. Xu: Proceedings of the 1998 ASME International Mechanical Engineering Congress and Exposition, **HTD-Vol. 361-4**, 79 (1998)
12. C.J. Knight: AIAA J. **17**, 519 (1979)
13. H.W. Liepmann, A. Roshko: *Elements of Gas Dynamics* (Wiley, New York 1973)
14. K.H. Song, X. Xu: Appl. Phys. A **65**, 477 (1997)
15. X. Xu, K.H. Song: J. Heat Transfer **119**, 502 (1997)
16. M.M. Martynyuk: Russian J. Phys. Chem. **57**, 494 (1983)